Mechanical Behavior and Numerical Estimation of Fracture Resistance of a SCS6 Fiber Reinforced Reaction Bonded Si_3N_4 Continuous Fiber Ceramic Composite

Oh-Heon Kwon*

Department of Safety Engineering, Pukyong National University, Busan 608-739, Korea

Michael G. Jenkins

Department of Mechanical Engineering, University of Washington, Seattle, WA98195, U.S.A

Continuous fiber ceramic composites (CFCCs) have advantages over monolithic ceramics : Silicon Nitride composites are not well used for application because of their low fracture toughness and fracture strength, but CFCCs exhibit increased toughness for damage tolerance, and relatively high stiffness in spite of low specific weight. Thus it is important to characterize the fracture resistance and properties of new CFCCs materials. Tensile and flexural tests were carried out for mechanical properties and the fracture resistance behavior of a SCS6 fiber reinforced Si_3N_4 matrix CFCC was evaluated. The results indicated that CFCC composite exhibit a rising R curve behavior in flexural test. The fracture toughness was about 4.8 MPa · $m^{1/2}$, which resulted in a higher value of the fracture toughness because of fiber bridging. Mechanical properties as like the elastic modulus, proportional limit and the ultimate strength in a flexural test are greater than those in a tensile test. Also a numerical modeling of failure process was accomplished for a flexural test. This numerical results provided a good simulation of the cumulative fracture process of the fiber and matrix in CFCCs.

Key Words : Continuous Fiber Ceramic Composite, Fracture Toughness, Fracture Resistance Behavior, Tensile and Flexural Test, Mechanical Properties, Numerical Modeling, Failure Process

1. Introduction

Recently there have been rapid developments for the industrial applications of some advanced ceramic composites. These composites are notable for their excellent mechanical properties. Specifically, composites consisting of advanced ceramic matrices such as silicon nitride reinforced with continuous ceramic fibers are overcoming many limitations caused by the brittleness of monolithic ceramics. These continuous fiber ceramic composites (CFCCs) have the same advantages of monolithic ceramics such as resistance to heat and resistance to erosion making them suitable for applications in chemical reactors, power generator, and engine. Furthermore, CFCCs have relatively high stiffness in spite of low weight. In addition, unlike their monolithic counterparts, CFCCs exhibit greatly increased toughness, which serves to decrease their inherent damage tolerance and increase their reliability.

Because of this increased reliance on toughness for damage tolerance, it is important to characterize the fracture resistance and material properties of new CFCCs materials. The development of complete database for CFCCs must be carried out in order for these materials to achieve their

---

* Corresponding Author,
  E-mail : kwon@pknu.ac.kr
  TEL : +82-51-620-1522; **FAX :** +82-51-620-1516
  Department of Safety Engineering Pukyong National University, San 100, Yongdang-Dong Nam-Gu, Busan 608-739, Korea. (Manuscript **Received** January 9, 2002; **Revised** June 10, 2002)

potential in numerous engineering applications.

A number of experimental investigations have conducted on the processing, properties and theories of matrix cracking, ultimate strength and toughness behaviors of CFCCs in particular fiber reinforced silicon nitride. For example, Danforth et al. (1983) studied for a number of properties, including fracture toughness of reaction bonded silicon nitride (RBSN) with various α/β ratio in 1983. Nair et al. (1991) examined initiation toughness and subsequent R curve behavior at elevated temperature using SCS6 fibre-reinforced RBSN. Xu et al. (1994) studied short crack mechanical properties and failure mechanism of SiC/Si$_3$N$_4$ composites by the indentation strength technique, applying this information to the R curve behavior of CFCCs. Jenkins et al. (1996) investigated the link between the macroscopically measured proportional limit stress in tension and the first cracking stress measured using acoustic emission techniques in a CFCCs. Bhatt (2000) measured the mechanical properties of SiC-fiber/RBSN and analyzed the composite microstructure. Raghuraman et al. (1996) modeled the flexural behavior of CFCC using finite element analysis model. They showed that the ordinary beam equations cannot be used to describe the behavior of laminated CFCCs. Van Landeghen and Jenkins (1999) also examined the utility of three ASTM standard test methods in developing precision and bias statements using Nicalon™ fiber/Si-C-O-N matrix (Sylramic™) CFCC. In spite of these investigations there are still major issues that need to be studied in order to obtain clear understanding of these CFCCs.

In this work, results are reported for tensile and flexural testing as well as numerical modeling of failure process for a SCS6 fiber reinforced Si$_3$N$_4$ matrix composites. An objective of this study was to obtain the basic of mechanical properties of a CFCC and link these to the fracture resistance behavior of the material.

2. Experimental Procedure

2.1 Material and specimens

The used material in this study was a commer-cial material comprised of unidirectional SCS6-fiber reinforcing Si$_3$N$_4$-matrix. Scanning electron microscope (SEM) was used to examine the microstructure of the material. To prepare SEM samples, test specimens of material were first sectioned normal to the fibers and then mounted in a red phenolic powder mold, grounded successively on #400 up to #1200 emery papers and polished in a vibratory polisher on a micro cloth using a 0.3 μm diamond powder paste. The mounted samples were coated with a thin layer of carbon in a vacuum evaporator to avoid charging during observation by SEM. Then the fiber diameter and their distribution were examined on the sample cross section normal to the fibers. Fiber distributions were uniform as shown in Fig. 1. The major diameter of the SCS6 fiber was 177.5 μm including a 1.76 μm thick carbon rich surface coating and 49.3 μm diameter carbon core.

Test specimens having straight-sided flat and reduced gage sections (i.e., dogbone) were prepared for tensile tests per ASTM C1275. The tensile test specimen configuration is shown in Fig. 2. End tabs adhered to the gripped section of the test specimen were used to protect the test specimens from being damaged from the closure of the hydraulically-actuated wedge grips. Clamping without using end tabs can produce localized damage due to the contact of the grip surface with the specimen. The end tabs were made
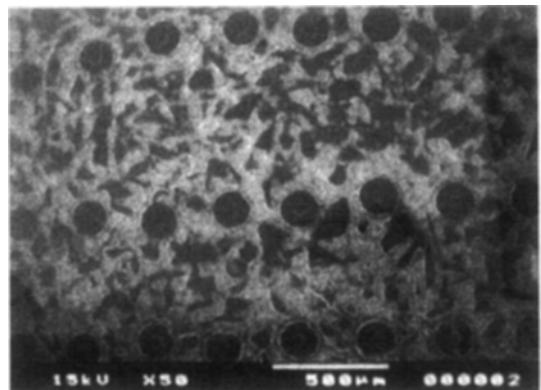

Fig. 1 The fiber distribution and configurations of SCS6 fiber/Si$_3$N$_4$ matrix composite by the SEM
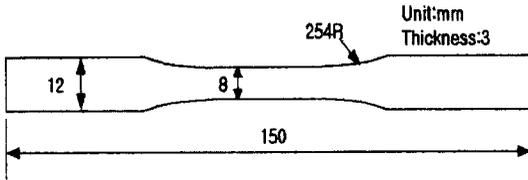
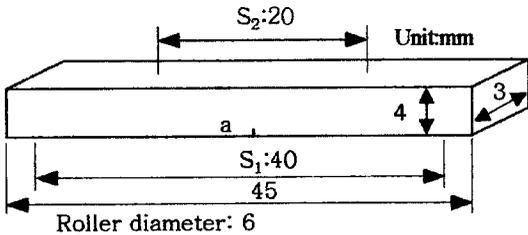**Fig. 2** The specimen configuration of the tensile test for CFCCs

Fig. 3 The specimen configuration of the flexural test

of E-glass fiber/epoxy matrix composites.

Flexural test specimens were also prepared for four-point flexure tests because the flexural properties are different from the tensile test properties. The flexure test specimens ($3 \times 4 \times 50$ mm as shown in Fig. 3) were machined by a conventional diamond-grit saw blade with 254 μm in thickness per specifications of ASTM Test Method C1341. For notched flexure tests, the notches were introduced with a diamond blade (254 μm thick). Notched flexure tests were conducted using the procedure for single edged precracked beams (SEPB contained in ASTM Test Method C1421). Both fracture toughness and fracture resistance were determined using the SEPB configuration with a notch depth to specimen height ratio of about 0.20.

2.2 Material properties

The density of materials was measured by the Archimedes techniques (1989) using distilled water as the immersion medium. The average bulk density of this $SCS6/Si_3N_4$ CFCC was determined to be 2.64 g/cm^3. The bulk porosity of the CFCC can be determined by first noting that the density of the matrix and the fiber was 3.26 g/cm^3 and 3.2 g/cm^3, respectively. The fiber volume fraction was estimated as 10.5% by

calculating areas of fibers section in the specimen with known cross sectional area connecting fiber section center points. The volume fraction of composite can be calculated:

$$\rho_c = \rho_m V_m + \rho_f V_f \qquad (1)$$

where ρ_c, ρ_m, ρ_f are the density of the composite, matrix and fiber, respectively, and V_m, V_f are the volume fractions of matrix and fiber, respectively. Using Eq. (1) and the respective constituent density, the volume fraction of matrix was calculated as 70.7%. The volume fraction of porosity is 18.8%.

2.3 Tensile test

Unnotched tensile specimens were used for measuring mechanical properties of elastic modulus, proportional limit stress, and ultimate tensile strength. Test specimens were loaded using an interchangeable, hydraulically actuated specimen grip system which can maintain an adjustable grip force without backlash and be independently activated. Gage section displacement for the calculation of strain was measured using an dual extensionmeter attached by spring force to the test specimen. For the dual extensionmeter, Axis A and Axis B were on the opposite faces of the gage section of the test specimen with 25 mm initial gage length and upper and lower strain ranges over the gage length of +5% to 2%, respectively. Strain was measured directly using a conventional, adhesively bonded electrical resistance strain gages.

All tensile tests were conducted at ambient temperature on a commercial single actuator electro mechanical materials test system having load, stroke, strain control capabilities. All signals during the tensile test were acquired by the digital controller and related software (superpack). Alignment was verified by measuring the strain on the four faces of only a strain gage dummy (steel) test specimen. The purpose of the verification procedure was to minimize the introduction of bending moments into the specimen during tensile test different from less 5% bending at an average strain of 500 μm/m in the alignment specimen. For displacement control,

test rates of 0.1 mm/s were used.

2.4 Flexural test

A custom four point flexural fixture was used for a flexural four-point bending test. The commercial test machine has force, displacement and strain control operation modes. Data acquisition and test control were performed from a digital controller using custom software package at a rate of 20 Hz. Testing was conducted in displacement control with a ramp rate of 0.1 mm/s. The test was continued until the total displacement was almost 1.5 mm.

3. Numerical analysis

3.1 Numerical model and properties

The numerical model simulation was based on the experimental conditions described previously in order to compare the numerical and experimental flexural results. An advantage of numerical modeling is that it can be used to evaluate the influence of material parameters and, in parti-

Table 1   The material properties used in the numerical model

Constituent	Volume fraction V (%)	Elastic modulus E (GPa)	Poisson's ratio ν	Ultimate strength Su (MPa)
SCS6 fiber	10.5	515	0.15	4200
Si₃N₄ matrix	70.7	150	0.22	275

Fig. 4   A Double mesh and the same displacement concept of the fiber and matrix at coincide node

cular, it can provide an understanding of the mechanics of flexural behavior of the unidirectionally-reinforced CFCC of this study. Numerical modeling was carried out by using a commercial finite element analysis (FEA) code ANSYS™5.4. The FEA model used the average dimension of the prismatic beams employed in the flexural experimental tests. The element type was an 8-noded quadrilateral element. The double mesh concept (Mark, 1996) was adopted to account for different material types without generating extra nodes. Using the double mesh concept, any load applied to any node of the fiber mesh, also affected the same node of the matrix mesh. The total numbers of elements and nodes were 4928 and 7760 respectively. An example of the FEA double mesh concept for a notched flexure test specimen is shown in Fig. 4. Assumed material properties used in the numerical model are shown in Table 1.

3.2 Numerical procedure

A nonlinear, incremental displacement-controlled loading sequence was applied to the FEA model such that a total displacement of 0.9 mm was accomplished in 25 steps. At the end of each displacement step, conditional statements were checked to ascertain if the maximum principal stress in the fiber or matrix elements had exceeded the fiber or matrix strengths, respectively (i.e., $\sigma_1 > S_{UT}$). When this condition was met in an individual element, the element was killed using the ANSYS "kill" command in which the element stiffness was reduced to a predetermined value (typically ~0 by 1×10^{-12}). The matrix and fibers support a limited stress. The double mesh approximates the load transfer which occurs when the matrix begins to crack. Once a matrix element reaches the critical stress, the element reduces the stiffness to near zero and the load is then transferred to the fiber element. Generally, the fiber elements carried the internal load when matrix elements had been killed. Graphically, killed elements are removed from the model, although, they are mathematically still present with a reduced stiffness. Fiber elements would carry more tensile load when the matrix elements were killed.

4. Results and Discussion

Figure 5 shows stress-strain curve from a tensile test. An engineering stress-strain response is important for obtaining and analyzing mechanical properties. In Fig. 5, the stress-strain curve was linear up to the proportional limit stress similar to many other materials. However, at strains greater than the proportional limit strain, the stress increased nonlinearly and at much a slower rate up to the ultimate tensile strength. This change in response means the proportional limit stress at the onset of nonlinearity represents the stress at matrix cracking and which indicates the onset of the cumulative damage process underlying the nonlinear stress strain curve. There are three methods in ASTM Test Method 1275 to determine the proportional limit. Using one of these methods, (deviation from linearity method) the proportional limit stress was determined as the point at which the difference between the actual stress and stress calculated as the product of the elastic modulus, E, and the actual strain was equal to 10%. The elastic modulus, E, was calculated using a least square linear regression method from the slope of the linear part of a stress strain curve from 0 to 15 MPa. In this study, the elastic modulus and a proportional limit were 153.2 GPa and 50.7 MPa,
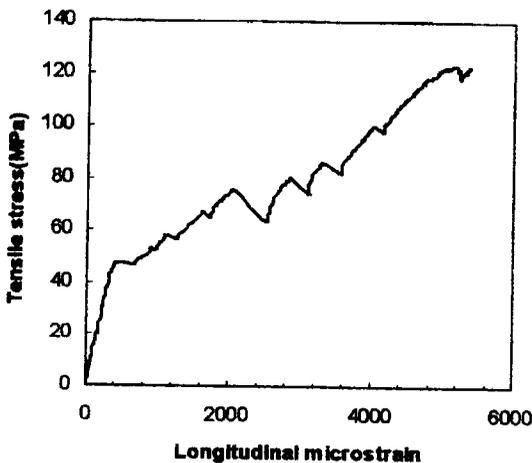
respectively. This implies that the first matrix cracking tensile strength is 50.7 MPa. The ultimate tensile strength was determined as 122 MPa.

Figure 6 shows an example of the typical load-displacement curve record from the four-point bending flexural test. The average ultimate flexure strength is 492 MPa which is considerably greater than the ultimate tensile strength. The elastic modulus in flexure was 182.5 GPa. The proportional limit stress in flexure (i.e., the first matrix cracking stress) was determined to be 180.8 MPa.

A predicted value of the first matrix cracking stress can be calculated using the relation of the Aveston, Kelly and Cooper (1971).

$$\sigma = \sigma_{mu}[1 + V_f(E_f/E_m - 1)] \qquad (2)$$

where σ_{mu} is the strength of the matrix (~ 150 MPa), V_f and V_m are the volume fractions of the fiber and matrix, E_f and E_m are the fiber and matrix moduli, respectively. Substituting values into Eq. (2) gives a predicted matrix cracking stress of 188.2 MPa.

In addition to these properties, the fracture toughness and fracture resistance behavior were evaluated from the SEPB fracture tests. A high toughness Silicon Nitride ceramic has been tested to experimentally verify that fracture resistance increases with crack propagation (so-called rising R curve behavior). Rising R-curve behavior can be related to stress relaxation in the
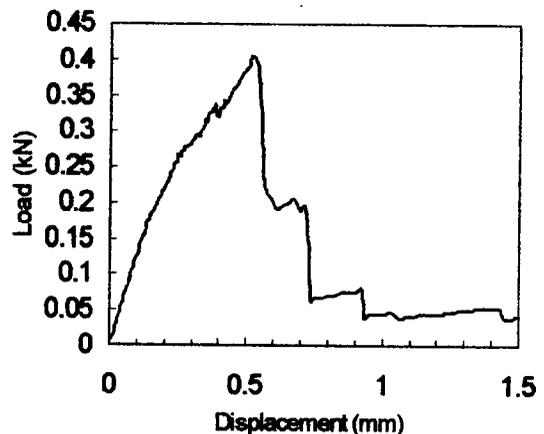

Fig. 5 A typical stress-strain curve acquired from a tensile test for SCS6 tiber/Si_3N_4 matrix

Fig. 6 An example of the load-displacement curve acquired from a flexural test for SCS6 fiber/Si_3N_4 matrix CFCCs

crack tip process zone. R–curves (i.e., increasing fracture resistance with crack extension) in CFCCs have not been evaluated yet.

To examine R curve behavior, the crack extension measurement is needed. One method of measuring crack extension is by observation of the crack during loading using a long distance traveling microscope. However, this method is not practically appropriate because it is difficult to measure crack extension accurately. A more common method to determine the crack extension, is the use of master compliance curves (Jenkins et al., 1987). This is the method used in the current study in which the compliance, $C(a)$, for the notched four-point flexure test was calculated such that (Munz et al., 1980):

$$C(a) = [9(S_1 - S_2)^2/2BW^2E']$$
$$[\int^a Y^2(a)\,da + (S_1 + 2S_2)/18W] \quad (3)$$

Where S_1, S_2 are the major and minor spans, respectively and W the height, B the width, a the normalized crack relative length, a/W, $E' = E/1 - \nu^2$, and $Y(a)$ the K calibration factor for a straight-through crack as follows:

$$Y(a) = 3(S_1 - S_2)\,\Gamma a^2/2(1-a)^{3/2} \quad (4)$$
$$\Gamma = 1.9887 - 1.326a(3.49 - 0.68a + 1.352a^2) \\ a(1-a)/(1+a)^2 \quad (5)$$

Figure 7 shows the master compliance curve for the crack relative length. The master compliance curve was used to determine the crack extension from the measured compliances of the load-displacement curve. Then by making a comparison between the compliance from Figs. 6 and 7, the crack extension can be found. The crack extension as a function of the load point is shown in Fig. 8. Then the crack growth resistance K_R was estimated during the stable crack propagation such that:

$$K_R = [P(S_1 - S_2)/BW^{3/2}]^{1/2}(3a^{1/2}Y/2) \quad (6)$$

Figure 9 shows R–curve behavior for the crack extension. The plateau value of K_R was estimated to be 16 MPa·m$^{1/2}$ and fracture toughness, K_{Ic} was about 4.8 MPa·m$^{1/2}$. The numerically-determined load versus displacement curve for the
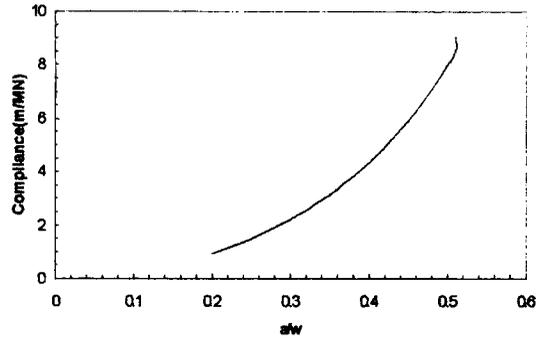

Fig. 7   The master compliance curve for the crack relative length, a/w
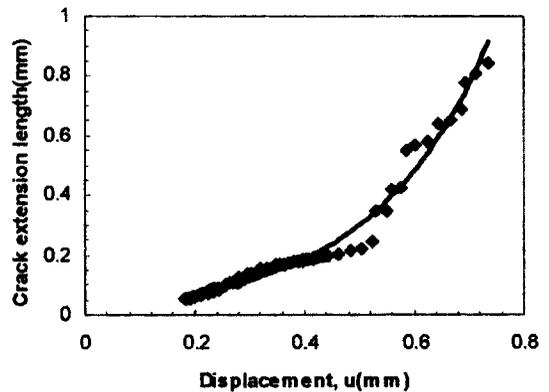

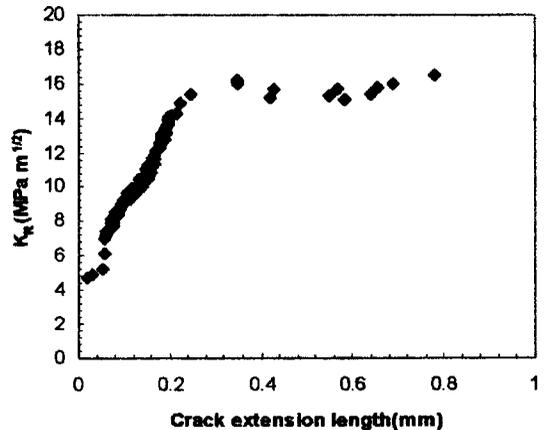Fig. 8   The crack extension variation according to the displacement in the flexural test

Fig. 9 K_R curve behavior for the crack extension

notched test specimen is shown in Fig. 10 along with experimental results for test specimens of approximately the same dimensions. The numerical result is a little different from the experimental

results in spite of the dimensional similarity and identical material. This difference may result from the inherent strength distribution characteristics of ceramic composites.

The numerical results seem to give an average approximation of the experimental load versus displacement curves after the first matrix cracking. There is a good agreement between the numerical model and the experimental results at
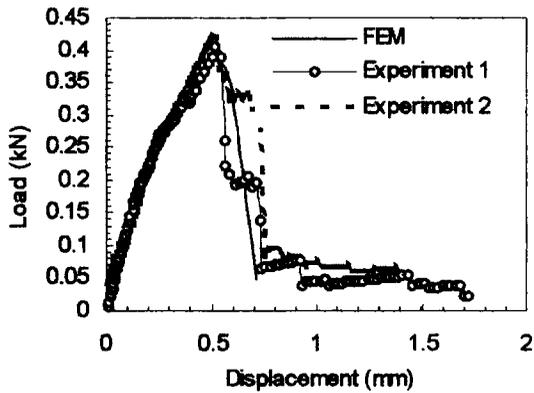

Fig. 10 The load-displacement curves from the numerical analysis

the first matrix cracking. Figures. 11(a) and 11 (b) show the respective stress distributions for the fiber and matrix elements at the first displacement step. In the elastic region, neither the fiber nor matrix stresses exceed critical stresses. Therefore, no killed elements are not shown in the model in the elastic region.

At the onset of the nonlinear behavior (i.e., matrix cracking) the first matrix elements are killed. In the nonlinear region after the first cracking, matrix failure continues and more matrix elements are killed. As elements are killed, the compliance of the model increases and the slope of the load-displacement curve decreases. At the maximum load, the first fiber elements are killed. This means fiber breaking begins at the ultimate strength.

During the unloading, more fiber elements are killed. As fibers fail, they transfer loads to other fibers and this lead to increasing stress on those fiber, thus increasing the possibility of failure. By the sixth displacement step, the first elements in the matrix have satisfied the failure criterion and the stiffness for these elements were reduced (i.e.,
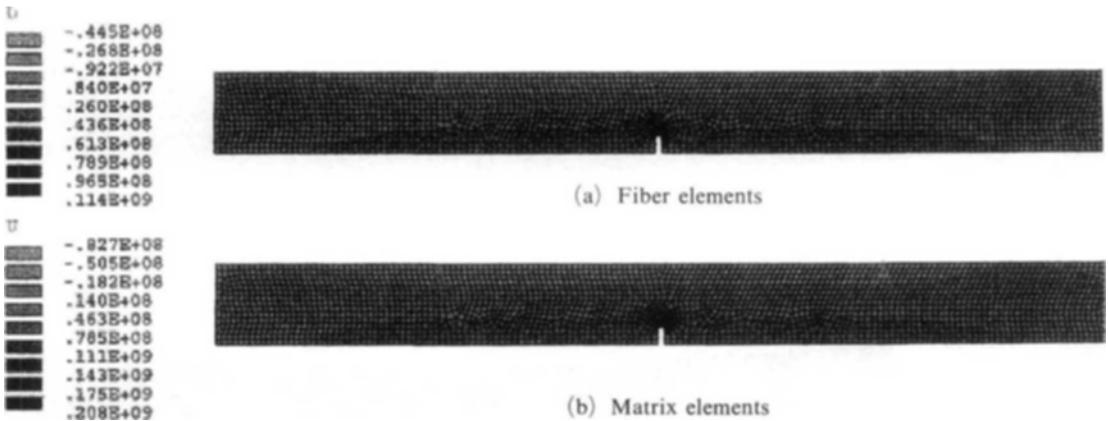

(a) Fiber elements

(b) Matrix elements

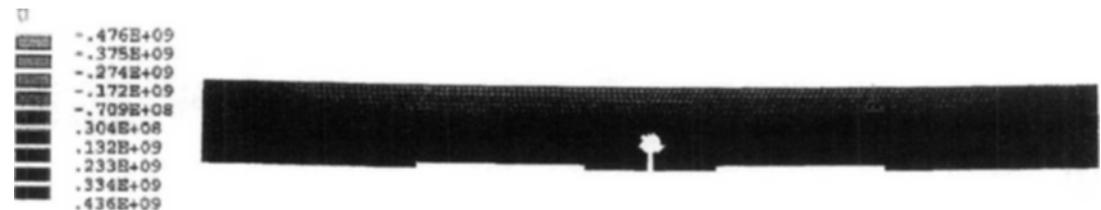Fig. 11 The stress distribution of the elements at the first loading displacement step

Fig. 12 The killed elements of the matrix at the sixth loading displacement step

killed elements) as shown in Fig. 12. Stresses are obviously increasing in the fiber elements at the location where the matrix elements are killed. Up until the sixteenth displacement step, the elements continue to be killed. These steps correspond to the nonlinear loading part on the load-displacement curve. On the seventeenth displacement step, some of the fiber elements have exceed the maximum strength and begin to be killed as shown in Fig. 13. The vertical displacement at the loading points is 0.53 mm correlating to the maximum load on the specimen. From this step until the last step, the fiber elements are killed as their element stresses exceed the maximum strength as shown in Figs. 14(a) and 14(b). Unlike that of the matrix elements, the pattern of the killed fiber elements does not spread longitudinally. At the last displacement step, many matrix elements are killed leaving few elements to support the load, although many fiber elements are left. Eventually, the remaining fibers prevent catastrophic failure and give rise to the graceful failure in the structure.

Here we would like to explain fracture propagation on strength mechanics respect and visualization using ANSYS birth and death element. However, some fracture criterions, K or others have to be used for the crack propagation. We will report the results using fracture criterion approach on the next paper.

5. Conclusions

The tensile and flexural empirical test results along with numerical modeling were conduced on SCS6-fiber/Si$_3$N$_4$-matrix composites. Several conclusions were obtained as follows.

(1) The elastic modulus, a proportional limit and the ultimate strength in a flexure test are greater than those in a tensile test.

(2) The empirical proportional limit gives almost same value to a predicted value of the first matrix cracking stress calculated by AKC equation.

(3) The plateau value of R-curve is estimated to be 16 MPa·m$^{1/2}$ and fracture toughness K$_{Ic}$ is about 4.8 MPa·m$^{1/2}$.

(4) Numerical results provided a good simu-

Fig. 13 The killed elements the fiber at the seventeenth loading displacement step

(a) Fiber elements
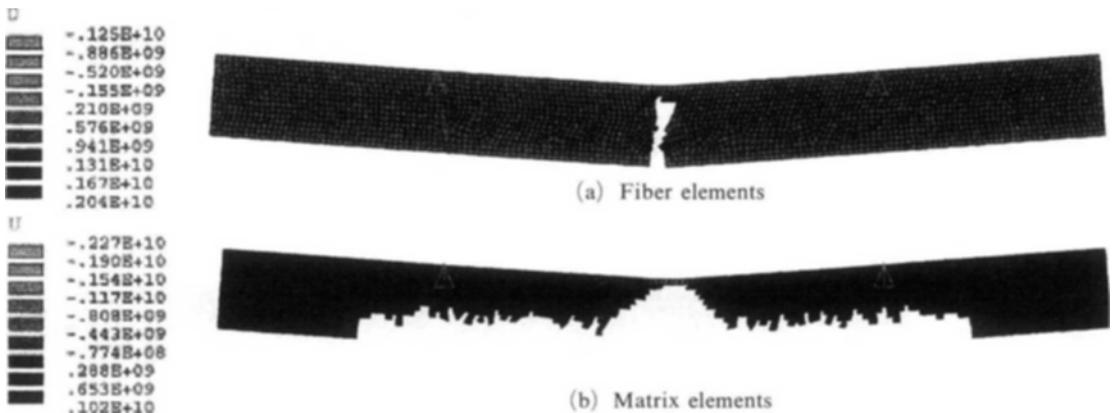
(b) Matrix elements

Fig. 14 The failure configuration of the elements at the last loading displacement step

lation of the cumulative failure processes of the fiber and matrix in 4 point bending specimen.

Acknowledgment

References

Danforth, S. C. and Richman, M. H., 1983, "Strength and Fracture Toughness of Reaction-Bonded Si_3N_4," *Am. Ceramic Soc., Bulletin*, Vol. 62, No. 4, pp. 501~504.

Nair, S. V., Gwo, T. J., Narbut, N. M. and Kohl, J. G., 1991, "Mechanical Behavior of a Continuousf - SiC - Fiber-Reinforced RBSN-Matrix Composites," *J. Am. Ceramic Soc.*, Vol. 74, No. 10, pp. 2551~2558.

Xu, H. H. K., Ostertag, C. P. and Braun, L. M., 1994, "Short-Crack Mechanical Properties and Failure Mechanism of Si_3N_4-matrix/Sic-Fiber Composites," *J. Am. Ceram. Soc.*, Vol. 77, No. 7, pp. 1889~1896.

Bhatt, R. T., 2000, "Tensile Properties and Microstructral Characterization of Hi-Niclon Sic/RBSN Composites", *Ceramic International*, Vol. 26, pp. 535~539.

Raghuraman, S., Lara-Curzio, E. and Ferber, M. K., 1996, "Modelling of Flexural Behavior of Continuous Fiber Ceramic Composites," *Ceram. Eng. & Sci. Proc.*, Vol. 17, No. 4, pp. 147~156.

Van Landeghen, P. L. and Jenkins, M. G., 1999, "Comparative Investigation of Intra and Inter Laboratory Mechanical Test of Flexural, Tensile and Shear Behavior CFCC," *Ceram. Eng. & Sci. Proc.*, Vol. 20, Issue3, pp. 605-613.

Pennings, E. C. M. and Grellner, W., 1989, "Precise Nondestructive Determination of the Density of Porous Ceramics," *J. Am. Ceram. Soc.*, Vol. 72, No. 2, pp. 1268~1270.

Mark, K. Y., 1996, "Numerical Modeling of the Mechanical Response of a Continuous Fiber Ceramic Composite in Flexure," MS Thesis, University of Washington.

Aveston, J., Cooper, G. A. and Kelly, A., 1971, "Single and Multiple Fracture in the Properties of Fiber Composites," *Proc. of the Nat. Physical Lab.*, IPC Sci. and Tech. Press.

Jenkins, M. G., Kobayashi, A. S., Sakai, M., White, K. W. and Bradt, R. C., 1987, "A 3-D Finite Element Analysis of a Chevron Notched Three Point Bend Fracture Specimen", *Int. J. of Fracture*, Vol. 34, pp. 281~295.

Munz, D., Bubsey, R. T. and Shannon, J. L., Jr., 1980, "Fracture Toughness Determination of Al_2O_3 Using Four-Point Bend Specimens with Straight-Through and Chevron Notches," J. Am. Ceram. Soc., Vol. 63, No. 5-6, pp. 300~305.